Journal of Applied Physics

Electronegative ligands enhance charge transfer to Mn_{12} single-molecule magnets deposited on graphene

Cite as: J. Appl. Phys. **127**, 064303 (2020); https://doi.org/10.1063/1.5128329
Submitted: 19 September 2019 . Accepted: 26 January 2020 . Published Online: 12 February 2020

Xiaochen Zhu, Ashlyn Hale, George Christou, and Arthur F. Hebard

Journal of Applied Physics ARTICLE scitation.org/journal/jap

Electronegative ligands enhance charge transfer to Mn_{12} single-molecule magnets deposited on graphene

Cite as: J. Appl. Phys. **127**, 064303 (2020); doi: 10.1063/1.5128329
Submitted: 19 September 2019 · Accepted: 26 January 2020 ·
Published Online: 12 February 2020

Xiaochen Zhu,[1] Ashlyn Hale,[2] George Christou,[2] and Arthur F. Hebard[1,a)]

AFFILIATIONS

[1]Department of Physics, University of Florida, Gainesville, Florida 32611, USA
[2]Department of Chemistry, University of Florida, Gainesville, Florida 32611, USA

[a)]**Author to whom correspondence should be addressed:** afh@phys.ufl.edu

ABSTRACT

Combining single-molecule magnets (SMMs) and emergent two-dimensional substrates such as graphene may lead to device configurations that are promising for spintronics and quantum computing. However, to fully exploit the unique features of SMMs anchored to two-dimensional substrates, the choice of ligand attachments, which could affect the magnetic and electronic properties, is critical. In this work, we focus on hybrid junctions comprising CVD-grown graphene and $[Mn_{12}O_{12}(O_2CR)_{16}(H_2O)_4]$(R = CH_3, $CHCl_2$) SMMs with different ligands. We find that $[Mn_{12}O_{12}(O_2CCH_3)_{16}(H_2O)_4]$ SMMs barely change the graphene's conductivity, while $[Mn_{12}O_{12}(O_2CCHCl_2)_{16}(H_2O)_4]$ SMMs with more electronegative ligands, by means of charge transfer, remarkably modify the electronic transport in graphene as revealed by gate-voltage dependent magnetotransport measurements.

I. INTRODUCTION

Monodisperse single-molecule magnets (SMMs), featuring long coherence times in combination with optical and electrical tunability, hold promise for information storage, quantum computing, and optoelectronic technologies.[1,2] $[Mn_{12}O_{12}(O_2CR)_{16}(H_2O)_4]$ SMMs serve as a promising platform for device prototype investigations due to their large ground state spin $S = 10$ and significant magnetic anisotropy.[3] Using established chemical methods, Mn_{12} derivatives can be synthesized with different ligands to tune various properties. Considerable efforts using surface sensitive techniques have been devoted to understanding the hybrid structures comprising Mn_{12} molecules deposited onto metallic (Bi, Au, Ni, Cu, Rh) as well as insulating (BN) substrates for the purpose of elucidating structural and electronic information required for device development.[4–7] In general, interfacial interaction between molecules and substrate, when understood and exploited properly, should facilitate achieving a synergistic combination of emergent properties and functionalities beyond the reach of the constituent materials alone.[8]

Semimetallic graphene promises to be a versatile candidate in the field of molecular spintronics due to its monolayer nature, unique Dirac spectrum, long spin diffusion length, gate tunable carrier density, and high carrier mobility.[9] Examples include adsorbate-induced doping for sensing applications,[10] attachment of $TbPc_2$ (Pc = phthalocyanine) SMMs to graphene nanoconstrictions for electrical detection of magnetization reversals,[11] use of thin-film and bulk graphitic samples to study SMM spin–substrate interactions,[12] and use of adatom-engineered graphene to detect local moments and spin flip scattering.[13] Herein, we focus on how Mn_{12} derivatives differing in the electronic properties of their carboxylate ligands affect the transport properties of graphene via SMM–substrate interactions. The ligands, in addition to protecting the inner Mn–oxo core, play an important role in coupling the molecules to their environment.[8,14] Specifically, density functional theory (DFT) calculations have shown that the interaction between Mn_{12} and graphene varies significantly with specific ligands, which serve as bridges for the transfer of electrons from graphene to Mn_{12}.[15] Accordingly, when interfacing with SMMs, we would expect graphene not only to act as a versatile and robust supporting layer but also to serve as an efficient probe that is sensitive to the electronic and magnetic properties of the molecules.

Herein, we report on a comparative transport study of graphene devices decorated by $[Mn_{12}O_{12}(O_2CR)_{16}(H_2O)_4]$ (R = CH_3, Mn_{12}-CH_3; R = $CHCl_2$, Mn_{12}-$CHCl_2$) SMMs. The

electronic response of the graphene remains essentially unchanged when covered with the Mn_{12}-CH_3 molecules, whereas the more electronegative Mn_{12}-$CHCl_2$ molecules attract considerably more electrons to hole dope the graphene. This charge transfer creates charge impurities that reside in the SMM overlayer and modify the graphene by reducing carrier mobilities, increasing charge inhomogeneity, and suppressing carrier phase coherence lengths/times.

II. METHODS

We start from commercially available (Graphene Supermarket) CVD-grown graphene on Si/SiO_2 (285 nm) wafers. Our graphene samples were etched into a Hall-bar structure as shown in Fig. 1(a) using an O_2 plasma. Here, the channel length is 40 μm and channel width is 15 μm. Electric contacts were defined by photolithography, followed by e-beam evaporation of Cr/Au (5 nm/40 nm) and lift-off in acetone. Prior to electrical measurements, the as-prepared graphene devices were vacuum ($<1 \times 10^{-6}$ Torr) annealed at 140 °C for 1.5 h to set the charge neutrality (Dirac) point (CNP) in the gate-voltage range of 20–30 V. Electrical measurements were carried out inside a Quantum Design PPMS with a magnetic field perpendicular to the sample plane. Magnetotransport data were obtained using a lock-in technique at 17.77 Hz, with excitation current less than 200 nA. Magnetic susceptibility was measured with a superconducting quantum interference device (SQUID).

Mn_{12}-CH_3 was prepared as previously described in the literature.[16] Following the well-established carboxylate ligand substitution procedure, Mn_{12}-$CHCl_2$ was synthesized from Mn_{12}-CH_3.[17] Mn_{12} SMM solutions (0.1 mM) were prepared by dissolving Mn_{12}-CH_3 and Mn_{12}-$CHCl_2$ crystals in acetonitrile. Immediately after measuring the pristine graphene device, ~50 nL of SMM solution was drop-cast over an approximate 4×4 mm^2 area on each device. Accordingly, the areal density of molecules is on the order of 2×10^{13} cm^{-2}. The decorated devices were then vacuum annealed at 140 °C for an additional hour to eliminate solvent residuals and to compensate for inadvertent air exposure, which can unintentionally p-dope the graphene and shift the CNP away from zero gate voltage.[18,19]

The robustness of the SMMs to 140 °C vacuum anneals was checked by depositing continuous films thick enough to span the 4–5 μm gaps of interdigitated gold electrodes deposited on insulating SiO_2 substrates. There was no difference in the temperature-dependent conductance of these samples measured over the temperature range from room temperature down to ≈150 K before and after annealing up to 140 °C. A second check on temperature sensitivity was made by vacuum annealing Mn_{12} crystals to 140 °C and observing no obvious degradation. In addition, since all of the graphene experiments were performed in an inert helium environment, there were no observed differences in electrical properties on temperature cycling.

Figures 1(b) and 1(c) show the temperature T dependence of the in-phase $\chi'(T)T$ and out-of-phase $\chi''(T)$ components of the magnetic susceptibility of Mn_{12}-$CHCl_2$ and Mn_{12}-CH_3 crystals at the indicated frequencies. Due to a significant magnetic anisotropy barrier, as T decreases, $\chi'(T)T$ exhibits a frequency-dependent roll-off with corresponding peaks in $\chi''(T)$ for both molecules. The second relaxation peaks near 2 K have been attributed to the Mn_{12} species containing an abnormally oriented Jahn–Teller axis.[20]

III. RESULTS AND DISCUSSION

A. Charge transfer

Figure 2 shows the dependence of conductivity σ on back gate voltage V_g measured at 5 K before and after doping with

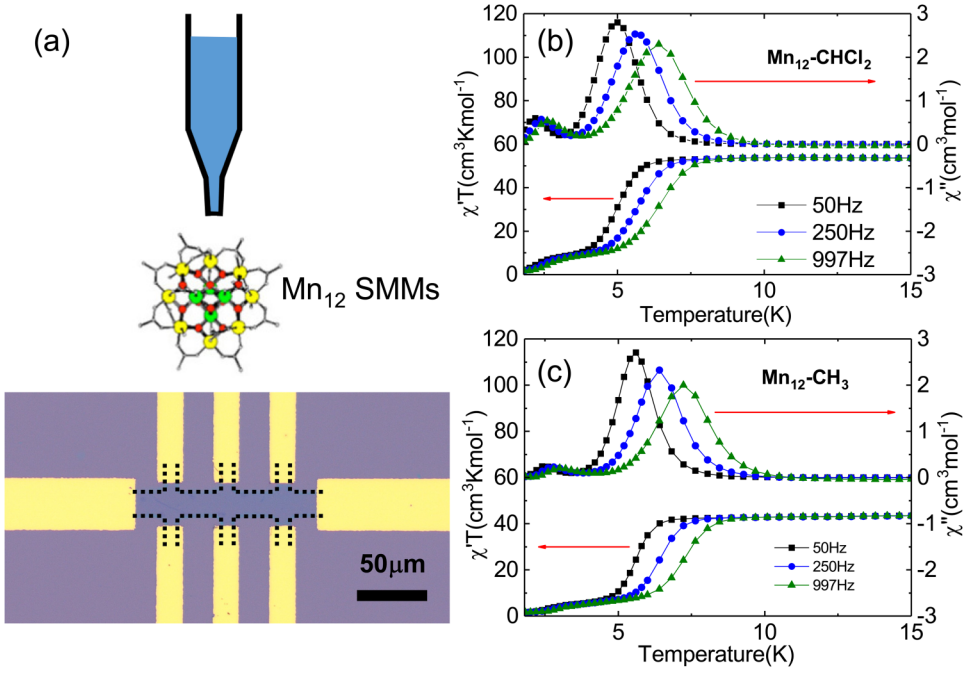

FIG. 1. (a) Drop casting schematics and the optical microscope image of Hall-bar graphene. In-phase and out-of-phase magnetic susceptibilities as a function of temperature for (b) Mn_{12}-$CHCl_2$ and (c) Mn_{12}-CH_3 crystals.

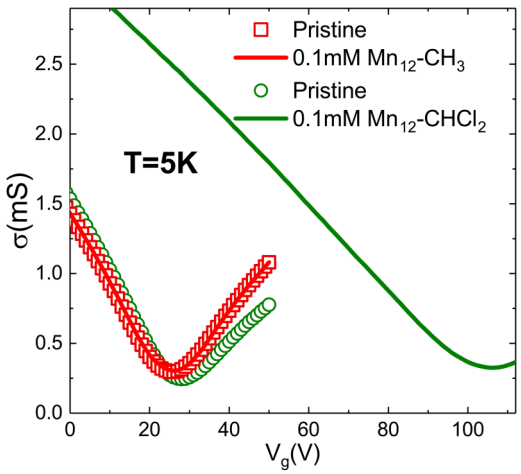

FIG. 2. Conductivity of graphene devices as a function of back gate voltages before and after molecule decoration measured at 5 K.

Mn_{12}-CH_3 or Mn_{12}-$CHCl_2$. Away from the Dirac point, conductivities of pristine and decorated graphene devices exhibit the typical linear dependence on carrier concentration, accompanied by a sublinear part at higher gate voltages, implying the coexistence of both long range and short range scattering processes.[21]

For graphene decorated with Mn_{12}-CH_3, the transfer curve almost overlaps with the pristine device, implying a negligible effect of molecules on the transport behavior of the underlying graphene. When the acetonitrile solvent alone is applied (Fig. 3), the transfer curve again almost overlaps with the pristine device, implying that the solvent has no effect on charge transfer. However, a dramatic shift of the Dirac point and a broadening of conductivity minima σ_{min} are observed in the Mn_{12}-$CHCl_2$ decorated devices. We note that for two out of the seven Mn_{12}-$CHCl_2$ decorated devices, the Dirac point shifts exceed 110 V, the approximate breakdown voltage of our SiO_2 gate oxide. Accordingly, the data are reproducible with all seven samples showing large CNP shifts. The average CNP shift of 70 V for the Mn_{12}-$CHCl_2$ dopant corresponds to an areal charge density $n = 5 \times 10^{12}\,\mathrm{cm}^{-2}$ calculated from $dn/dV_g = e^{-1}C$ for a gate capacitance $C = 1.21 \times 10^{-4}\,\mathrm{Fm}^{-2}$. Negligible charge transfer is observed for Mn_{12} with the less electronegative CH_3 ligand.

To make a qualitative assessment of the dependence of the CNP shift on Mn_{12}-$CHCl_2$ solution concentration, we applied a 0.035 mM Mn_{12}-$CHCl_2$ concentration and found a Dirac point shift of approximately 1/2 of the shift corresponding to the 0.10 mM concentration, as shown in Fig. 3. We conclude that the Dirac point and transfer curve do show a shift roughly in proportion to the concentration of the SMM molecules in the solution used for doping.

Figure 4 summarizes the CNP shifts together with mobility changes induced by charge transfer associated with ligand-dependent Mn_{12} doping. The plots are based on five graphene devices covered by Mn_{12} SMMs for each type of ligand with Dirac points located within our measurement range. Electron/hole mobility, calculated from the linear dependencies outside the CNP region using $\mu = e^{-1}(d\sigma/dV_g)(dV_g/dn)$, reveals a pronounced electron/hole asymmetry with the holes of the Mn_{12}-$CHCl_2$ samples (rightmost blue diamond) having a mobility lowered by about a factor of two due to the presence of charged impurities.

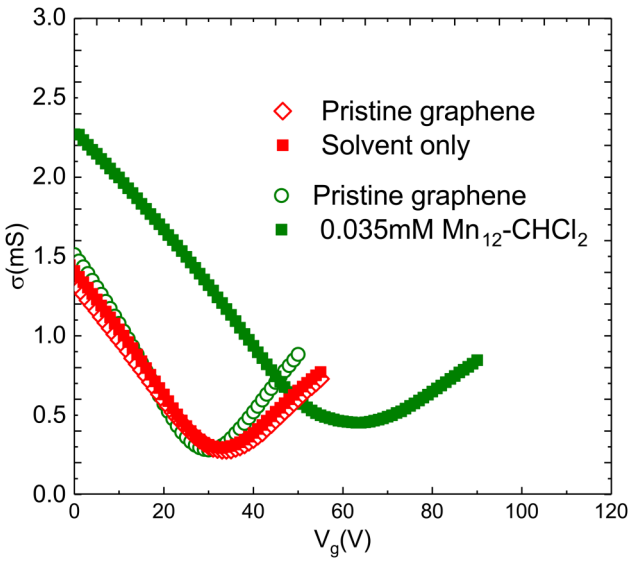

FIG. 3. Conductivity data of graphene decorated with acetonitrile (red) and 0.035 mM Mn_{12}-$CHCl_2$ solutions (green) at 5 K.

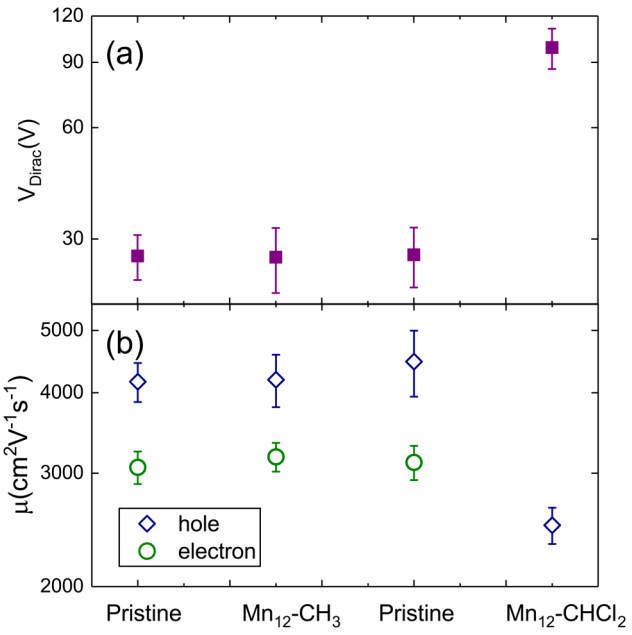

FIG. 4. Statistics for five sample pairs of the (a) Dirac point position and (b) carrier mobility extracted from transfer curves of both pristine and decorated graphene devices.

For pristine graphene, the initial Dirac point after annealing typically sits between 20 and 30 V. The extracted carrier mobilities show pronounced electron–hole asymmetry with $\mu_h \sim 4000$–$5000\,\mathrm{cm^2\,V^{-1}\,s^{-2}}$ and $\mu_e \sim 3000$–$3500\,\mathrm{cm^2\,V^{-1}s^{-2}}$. After coverage by Mn_{12}-CH_3 molecules, the Dirac point of graphene remains almost unchanged with even a slight enhancement of carrier mobility. This enhancement is due to additional vacuum annealing that helps release corrugations, ripples, and adsorbates.[19] We note that, according to the DFT calculations, graphene donates around 0.7 electrons to each Mn_{12}-$CHCl_2$ molecule.[15] The $5 \times 10^{12}\,\mathrm{cm^{-2}}$ electron transfer calculated from the CNP shift in Fig. 2, therefore, corresponds to a molecule coverage of around $7 \times 10^{12}\,\mathrm{cm^{-2}}$. Our previously described estimate from the concentration and volume of our doping solutions gives a molecule density of $\approx 2 \times 10^{13}\,\mathrm{cm^{-2}}$. Aggregation and various orientations of molecules account for this factor of three suppression of doping efficiency.[4,22] This interpretation is validated by a comparison of the AFM images of Fig. 5, showing the difference between pristine and the Mn_{12}-$CHCl_2$ covered graphene. We note that the clustering and additional roughness, although present, only mitigate the effect of charge transfer and does not affect our conclusions about the role of ligand attachments to the SMMs at the interface.

The Hall resistance measurements in Fig. 6, plotted as R_H vs gate-voltage difference $\Delta V_g = V_g - V_{CNP}$ for Mn_{12}-CH_3 (panel a) and Mn_{12}-$CHCl_2$ (panel b), reveal a pronounced crossover from conductivity dominated by holes to conductivity dominated by electrons as ΔV_g increases through zero at the CNP. For ideal graphene, R_H is given by $\pm 1/(en)$, where n is the carrier concentration, which diverges near the CNP. However, in the presence of non-negligible residual carrier densities (electron–hole puddles), $R_H = dR_{xy}/dB$ of graphene usually shows a less pronounced transition across the CNP, accompanied by a broadening of σ_{min}.[23,24] This crossover region is considerably broadened for the Mn_{12}-$CHCl_2$ dopants. As demonstrated by the dotted lines in Fig. 6, we fit the $R_H - V_g$ curves with Gaussian convolution with the standard deviation as an estimate of the residual carrier concentrations. This broadened region is suggestive of a higher density of electron/hole puddles near σ_{min}. The residual carrier concentration of the pristine devices is in the range of 4–$6 \times 10^{11}\,\mathrm{cm^{-2}}$, consistent with the previously reported values for CVD-grown graphene.[25]

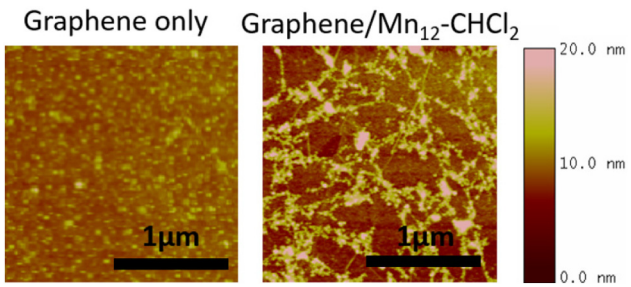

FIG. 5. AFM image of a typical annealed pristine graphene device before (left) and after Mn_{12}-$CHCl_2$ molecule coverage (right). After drop casting, the average surface roughness increases from 0.5 nm to 2.69 nm, implying aggregation and clustering of single-molecule magnets.

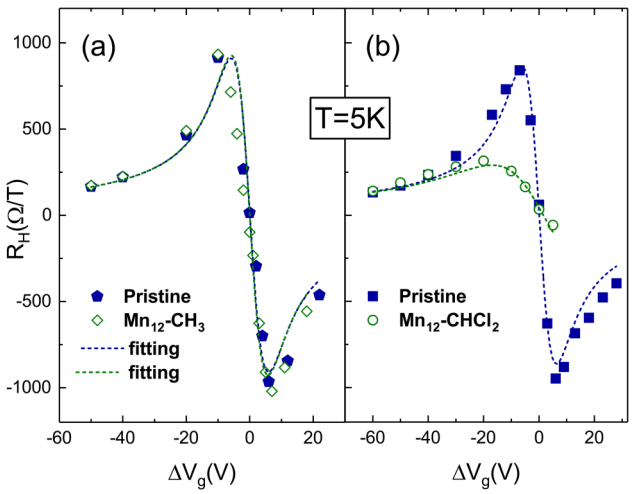

FIG. 6. Comparison of Hall resistances at 5 K as a function of gate voltages between pristine graphene and (a) Mn_{12}-CH_3 and (b) Mn_{12}-$CHCl_2$ decorated graphene. Dashed lines are the Gaussian convolution fitting.

The change induced by Mn_{12}-CH_3 molecules is within the error bar, while the residual carrier density rises to $1.4 \times 10^{12}\,\mathrm{cm^{-2}}$ when covered by Mn_{12}-$CHCl_2$ molecules (orange diamonds).

An additional method to quantify charged impurity disorder is to fit the transfer curves with the model proposed by Adam *et al.*[26,27] Away from the Dirac point, where $n > n^*$, $\sigma(n) = C_\sigma(n/n_i)$, while near the Dirac point, where $n < n^*$, $\sigma(n) = C_\sigma(n^*/n_i)$. Here, n is the carrier concentration, n_i is the charged impurity density, n^* is the density of the residual carriers, and the constant C_σ is calculated to be $20e^2/h$ for graphene on SiO_2 substrates. Within this framework, we plot in Fig. 7: $n_i = (20e^2/h)(d\sigma/dn)^{-1}$ (blue squares) and $n^* = n_{residual} = \sigma_{min}(d\sigma/dn)^{-1}$ (green circles).

The residual carrier densities obtained from the transfer curves and the Hall effect are generally in agreement with each other. However, we note that the charged impurity density induced by Mn_{12}-$CHCl_2$ obtained from transfer curves is in the range of 1–$2 \times 10^{12}\,\mathrm{cm^{-2}}$, only one fourth of the value estimated from the shift of the Dirac point. We attribute the discrepancy to the underestimation of the constant C_σ. The assignment $C_\sigma = 20e^2/h$ applies to the situation where the distance d between the graphene plane and the charged impurity layer is zero.[27] However, according to the DFT calculation,[15] electrons from graphene mainly transfer to Mn atoms instead of the ligand. Accordingly, the Mn_{12}-$CHCl_2$ molecules should be treated as remote charged scatterers sitting over 1 nm above the graphene. The underestimation originates from the diminished influence of remote charged impurities with $C_\sigma(d, n)$ increasing dramatically as the distance d becomes larger.[27]

B. Magnetotransport

Compared to transfer curves, the transport characteristics of graphene under magnetic field offer more detailed information regarding different scattering processes. As shown in Fig. 8, magnetoconductivities (MCs) of graphene manifest typical weak

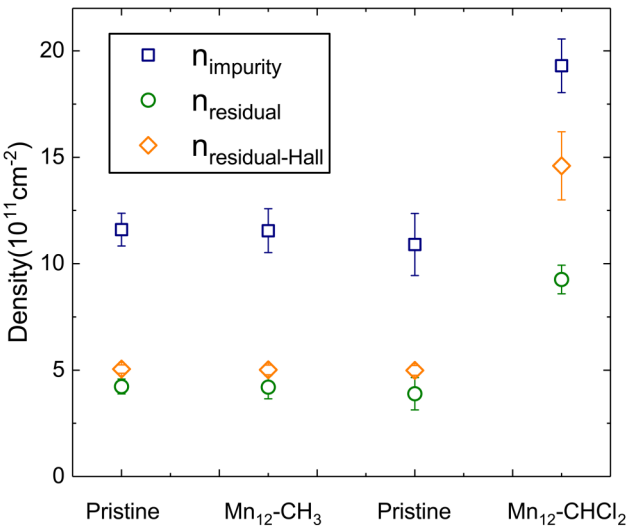

FIG. 7. Plot of impurity densities and estimated residual carrier (electron–hole puddle) concentrations from both transfer curves and Hall resistance fitting.

localization behavior, which emerges due to the appearance of intravalley and intervalley scatterings originating from chiral symmetry breaking by surface ripples, atomic-sized defects, etc.[28] We find that MC curves show negligible change with coverage of Mn_{12}-CH_3 molecules as shown in Fig. 8. However, Mn_{12}-$CHCl_2$ show noticeable changes in the MC traces with weak localization suppressed far away from the Dirac point and enhanced near the Dirac point.

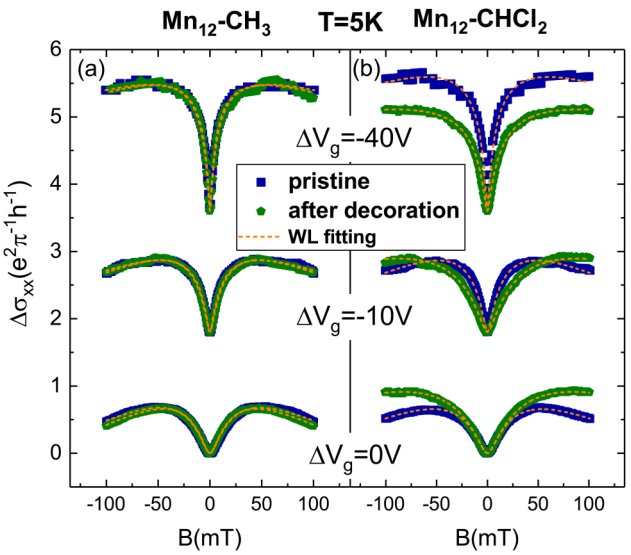

FIG. 8. Low field magnetoconductivity comparisons at 5 K of graphene before and after (a) Mn_{12}-CH_3 and (b) Mn_{12}-$CHCl_2$ molecule deposition near and away from the Dirac point.

We fit the MC curves with the McCann model,[29]

$$\Delta\sigma_{xx} = \frac{e^2}{\pi h} \times \left[\mathrm{F}\left(\frac{4eB/\hbar}{L_\phi^{-2}}\right) - \mathrm{F}\left(\frac{4eB/\hbar}{L_\phi^{-2} + 2L_i^{-2}}\right) - 2\mathrm{F}\left(\frac{4eB/\hbar}{L_\phi^{-2} + L_i^{-2} + L_*^{-2}}\right)\right], \quad (1)$$

$$\mathrm{F}(z) = \ln(z) + \psi(0.5 + z^{-1}),\ L_{\phi,i,*}^2 = D\tau_{\phi,i,*}, \quad (2)$$

where B is the perpendicular magnetic field, ψ is the digamma function, $L_{\phi,i,*}(\tau_{\phi,i,*})$ are the phase coherence length (time), intervalley scattering length (time), and intravalley scattering length (time), respectively. $D = v_F^2\tau/2$ is the diffusion constant, where v_F is the Fermi velocity and τ is the transport scattering time, which is the shortest of all the characteristic times.

As shown in Fig. 9(a), as n decreases ($\Delta V_g \to 0$), both L_ϕ and L_i decrease, whereas L_* shows a slight increase. After Mn_{12}-$CHCl_2$ deposition, L_*, L_ϕ, and L_i decrease at large gate voltages primarily because of the reduced carrier mobilities shown in Fig. 4. However, upon approaching the Dirac point, the differences gradually vanish. We attribute the diminishing difference to the existence of electron–hole puddles. The diffusion constant D, especially near the Dirac point, is affected by the presence of the charge impurity induced spatial carrier density fluctuations. We thus expect a larger actual diffusion constant near the Dirac point for decorated graphene due to a higher density of puddles. Accordingly, an enhanced diffusion constant compensates for SMM induced suppression of the characteristic lengths.

To obtain meaningful scattering times $\tau_{\phi,i,*}$, we focus on the back gate voltages from −30 V to −60 V, where the effect of

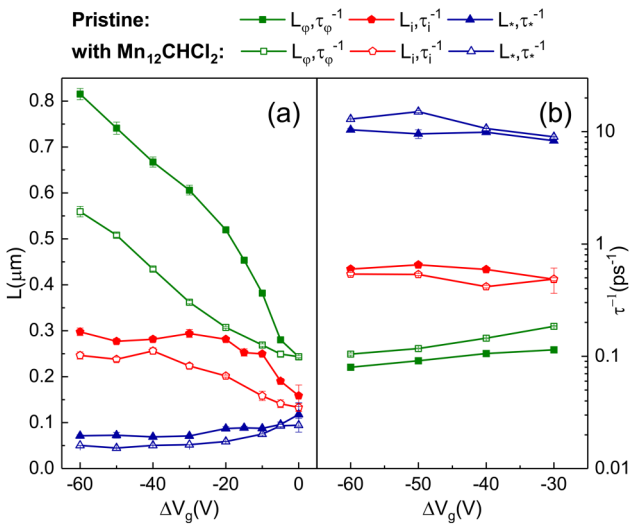

FIG. 9. (a) Extracted phase coherence lengths L_ϕ, intervalley scattering lengths L_i, and intravalley scattering lengths L_* as a function of gate voltages. (b) Extracted characteristic scattering rates far away from the Dirac point.

electron–hole puddles is negligible as evidenced by the overlap of Hall resistance in that range. As shown in Fig. 9(b), the major influence due to the introduction of Mn_{12}-$CHCl_2$ molecules is the increase in the phase breaking rate τ_ϕ^{-1}. Since our devices are in the "dirty limit" where $k_BT\tau/\hbar < 1$, the main source of dephasing comes from Nyquist scattering where electrons are scattered by the fluctuating electromagnetic fields generated by their neighbors:[30,31] $1/\tau_N \propto (k_BT/\hbar)\ln(g)/g$, where $g = \sigma h/e^2$. Thus, the transport scattering rate or conductivity mainly determines the phase breaking rate. Since the Mn_{12}-$CHCl_2$ overlayer reduces conductivity and increases transport scattering rates, an enhanced phase breaking rate is expected. Compared to τ_ϕ^{-1}, the changes of τ_i^{-1} and τ_*^{-1} are less pronounced, and at some gate voltages, the changes are within error bars. The slightly reduced τ_i^{-1} can be understood as a lower mobility that limits the chances of carriers scattered by either the atomically sharp defects or the sample edges.[28,32] The intravalley scattering rate τ_*^{-1} is mainly due to trigonal warping and long range charged impurity scattering. However, trigonal warping only matters at high carrier concentrations and decreases as mobility diminishes.[29,33] Accordingly, increased intravalley scattering results from a stronger long range Coulomb scattering with the coverage of Mn_{12}-$CHCl_2$ molecules.[34]

Although the absolute values of characteristic lengths and times are sample-dependent, all of our measured samples demonstrate similar features. Attribution of an enhanced phase breaking rate due to the spin-flip of Mn_{12} cores that possess a large spin center[13] with $S = 10$ is not plausible since the phase breaking rate remains virtually unchanged when the five Mn_{12}-CH_3 doped samples are compared with the pristine graphene samples. We attribute the absence of such spin-flip effects to the low dosage of molecules together with the large separation between the Mn cores and graphene plane. In addition, significant disorder/impurities pre-existing in our "pristine" CVD-grown graphene could mask the effect of spin-flip as well.

IV. CONCLUSIONS

By comparing the transport properties of graphene devices before and after Mn_{12} SMM decoration, we have highlighted the importance of ligands on the interfacial interaction and thus the electronic properties of SMM/graphene hybrid structures. We anticipate that SMMs with tailored ligands can serve as novel platforms to study spin-charge effects and uncover emergent phenomena with new functionalities when forming hybrid structures with abundant two-dimensional substrates.

ACKNOWLEDGMENTS

The authors thank Yunxi Liu, Haoming Jin, Preet Mahalay, and Sima Saeidi Varnoosfaderani for technical assistance and Hai-Ping Cheng for useful discussions. This work was supported as part of the Center for Molecular Magnetic Quantum Materials (M^2QM), an Energy Frontier Research Center funded by the U.S. Department of Energy, Office of Science, Basic Energy Sciences under Award No. DE-SC0019330.

REFERENCES

[1]L. Bogani and W. Wernsdorfer, Nat. Mater. **7**, 179 (2008).
[2]S. V. Aradhya and L. Venkataraman, Nat. Nanotechnol. **8**, 399 (2013).
[3]R. Bagai and G. Christou, Chem. Soc. Rev. **38**, 1011 (2009).
[4]K. Sun, K. Park, J. Xie, J. Luo, H. Yuan, Z. Xiong, J. Wang, and Q. Xue, ACS Nano **7**, 6825 (2013).
[5]S. Voss, M. Fonin, U. Rüdiger, M. Burgert, U. Groth, and Y. S. Dedkov, Phys. Rev. B **75**, 045102 (2007).
[6]K. Park, Phys. Rev. B **83**, 064423 (2011).
[7]S. Kahle, Z. Deng, N. Malinowski, C. Tonnoir, A. Forment-Aliaga, N. Thontasen, G. Rinke, D. Le, V. Turkowski, T. Rahman, S. Rauschenbach, M. Ternes, and K. Kern, Nano Lett. **12**, 518 (2012).
[8]M. Cinchetti, V. A. Dediu, and L. E. Hueso, Nat. Mater. **16**, 507 (2017).
[9]W. Han, R. K. Kawakami, M. Gmitra, and J. Fabian, Nat. Nanotechnol. **9**, 794 (2014).
[10]T. O. Wehling, K. S. Novoselov, S. V. Morozov, E. E. Vdovin, M. I. Katsnelson, A. K. Geim, and A. I. Lichtenstein, Nano Lett. **8**, 173 (2008).
[11]A. Candini, S. Klyatskaya, M. Ruben, W. Wernsdorfer, and M. Affronte, Nano Lett. **11**, 2634 (2011).
[12]C. Cervetti, A. Rettori, M. Gloria Pini, A. Cornia, A. Repollés, F. Luis, M. Dressel, S. Rauschenbach, K. Kern, M. Burghard, and L. Bogani, Nat. Mater. **15**, 164 (2016).
[13]X. Hong, K. Zou, B. Wang, S. H. Cheng, and J. Zhu, Phys. Rev. Lett. **108**, 226602 (2012).
[14]D. W. Boukhvalov, V. V. Dobrovitski, P. Kogerler, M. Al-Saqer, M. I. Katsnelson, A. I. Lichtenstein, and B. N. Harmon, Inorg. Chem. **49**, 10902 (2010).
[15]X.-G. Li, J. N. Fry, and H.-P. Cheng, Phys. Rev. B **90**, 125447 (2014).
[16]T. Lis, Acta Crystallogr. B **36**, 2042 (1980).
[17]M. Soler, P. Artus, K. Folting, J. C. Huffman, D. N. Hendrickson, and G. Christou, Inorg. Chem. **40**, 4902 (2001).
[18]H. Sojoudi, J. Baltazar, C. Henderson, and S. Graham, J. Vac. Sci. Technol. B **30**, 041213 (2012).
[19]A. Pirkle, J. Chan, A. Venugopal, D. Hinojos, C. W. Magnuson, S. McDonnell, L. Colombo, E. M. Vogel, R. S. Ruoff, and R. M. Wallace, Appl. Phys. Lett. **99**, 122108 (2011).
[20]S. M. J. Aubin, Z. M. Sun, H. J. Eppley, E. M. Rumberger, I. A. Guzei, K. Folting, P. K. Gantzel, A. L. Rheingold, G. Christou, and D. N. Hendrickson, Inorg. Chem. **40**, 2127 (2001).
[21]S. Das Sarma, S. Adam, E. H. Hwang, and E. Rossi, Rev. Mod. Phys. **83**, 407 (2011).
[22]E. Coronado, A. Forment-Aliaga, F. M. Romero, V. Corradini, R. Biagi, V. de Renzi, A. Gambardella, and U. del Pennino, Inorg. Chem. **44**, 7693 (2005).
[23]J. Martin, M. Akerman, G. Ulbricht, T. Lohmann, J. H. Smet, K. von Klitzing, and A. Yacoby, Nat. Phys. **4**, 144 (2007).
[24]E. A. Henriksen, D. Nandi, and J. P. Eisenstein, Phys. Rev. X **2**, 011004 (2012).
[25]M.-Y. Li, C.-C. Tang, D. C. Ling, L. J. Li, C. C. Chi, and J.-C. Chen, J. Appl. Phys. **114**, 233703 (2013).
[26]S. Adam, E. H. Hwang, V. M. Galitski, and S. Das Sarma, Proc. Natl. Acad. Sci. U.S.A. **104**, 18392 (2007).
[27]E. H. Hwang, S. Adam, and S. Das Sarma, Phys. Rev. Lett. **98**, 186806 (2007).
[28]D. Ki, D. Jeong, J. Choi, H. Lee, and K. Park, Phys. Rev. B **78**, 125409 (2008).
[29]E. McCann, K. Kechedzhi, V. I. Fal'ko, H. Suzuura, T. Ando, and B. L. Altshuler, Phys. Rev. Lett. **97**, 146805 (2006).
[30]F. V. Tikhonenko, A. A. Kozikov, A. K. Savchenko, and R. V. Gorbachev, Phys. Rev. Lett. **103**, 226801 (2009).
[31]B. L. Altshuler, A. G. Aronov, and D. E. Khmelnitsky, J. Phys. C **15**, 7367 (1982).
[32]F. V. Tikhonenko, D. W. Horsell, R. V. Gorbachev, and A. K. Savchenko, Phys. Rev. Lett. **100**, 056802 (2008).
[33]A. M. R. Baker, J. A. Alexander-Webber, T. Altebaeumer, T. J. B. M. Janssen, A. Tzalenchuk, S. Lara-Avila, S. Kubatkin, R. Yakimova, C.-T. Lin, L.-J. Li, and R. J. Nicholas, Phys. Rev. B **86**, 235441 (2012).
[34]J. Moser, H. Tao, S. Roche, F. Alzina, C. M. Sotomayor-Torres, and A. Bachtold, Phys. Rev. B **81**, 205445 (2010).